

Article

Correlative Impact of Shading Strategies and Configurations Design on Pedestrian-Level Thermal Comfort in Traditional Shophouse Neighbourhoods, Southern China

Shi Yin ^{1,2} , Werner Lang ³, Yiqiang Xiao ^{1,2,*} and Zhao Xu ⁴

¹ School of Architecture, South China University of Technology, Guangzhou 510641, China; yinshity@gmail.com

² State Key Laboratory of Subtropical Building Science, South China University of Technology, Guangzhou 510640, China

³ Institute of Energy Efficient and Sustainable Design and Building, Technical University of Munich, 80333 Munich, Germany; w.lang@tum.de

⁴ School of Civil Engineering, Southeast University, Nanjing 210096, China; xuzhao@seu.edu.cn

* Correspondence: yqxiao@scut.edu.cn

Received: 27 January 2019; Accepted: 27 February 2019; Published: 5 March 2019



Abstract: Traditional shophouse neighbourhoods (TSNs) in southern China respond well to the local hot and humid climate through proper street configurations and the integration of different shading strategies. Investigating the impact of shading strategies and configurations in TSNs on outdoor thermal comfort is valuable for guiding current urban design. Three street canyons in a TSN of Guangzhou with different shading strategies were selected as basic cases for microclimatic measurement in the summer season, i.e., alleys, streets with arcade for pedestrians, and streets with high-density greenery. After validating their simulation models in ENVI-met, five groups of parametric simulations were generated by varying the canyon aspect ratio (CHW), the canyon axis orientation, arcade proportion (AHW), and the tree-covered area (TCA). Using the physiological equivalent temperature (PET) to assess the above results, the correlative impact of different variations on pedestrian's thermal comfort and their corresponding favourable ranges are summarized. The findings suggest that: (a) only in alleys and arcade streets, the pedestrian-level thermal comfort was significantly influenced by canyon axis orientation. (b) The thermal stress for pedestrians increased dramatically when the CHW was lower than 1.5 in alleys and 0.78 in boulevards (in TCA = 89%), while the CHW higher than 1 indicated a remarkable reduction on the PET for pedestrians in arcades. (c) The pedestrians started losing the protection from shading strategy to thermal stress when the AHW was higher than 1.33 (in canyon with CHW = 1) or the TCA was lower than 33% (in canyon with CHW = 0.78).

Keywords: hot and humid climate zone; street canyon; shading strategy design; parametric simulation; pedestrian-level thermal comfort

1. Introduction

In recent decades, global warming has deteriorated the urban outdoor environment and has become a threat to the public health of residents, especially in areas with hot climates [1]. Due to the urgency of such matters, climate-resilient measures need be applied in the public realm to strengthen the adaptability of the outdoor environment to climate change and to maintain comfortable environments for pedestrians [2]. Regarding these measures, traditional neighbourhoods and

architectures have the potential to be a proper reference for responding to local climate after long-term historical accumulation [3] and is worth comprehensive study and implementation for contemporary urban design.

1.1. Traditional Shophouse Neighbourhoods (TSNs) and Local Climate

In southern China and southeast Asia, a special traditional neighbourhood (Figure 1), named traditional shophouse neighbourhood (TSN), can be found in most old quarter with semi-open arcades [4,5]. These neighbourhoods consist of two- to four-story townhouses with large depths and small widths, a shop with a semi-open arcade on the ground floor facing the main road, and a residence above the shop with a small patio [6]. The locations of TSNs are in areas with hot and humid climates that suffer extremely high thermal stress and frequent rain in the (rather long) summer season. Figure 1b illustrates climate information in Guangzhou (23.1° N, 113.3° E). From May to October, the average air temperature was over 25 °C and the maximum temperature was never lower than 33 °C; meanwhile, the average relative humidity was high, varying between 60% and 75%. In contrast, during the winter period, the weather was relatively warm and dry, with an average air temperature that was still over 15 °C (from November to April). Therefore, the main challenge for outdoor thermal comfort in this area is the long summer season with high thermal stress. The prevailing wind in Guangzhou is mainly from the north direction in winter and the southeast direction in summer. For ameliorating thermal stress in this area, three common shading strategies are integrated in the street canyon of TSNs to optimize pedestrian thermal comfort: shading from high aspect ratios, semi-open verandas for pedestrians, and tree canopies.

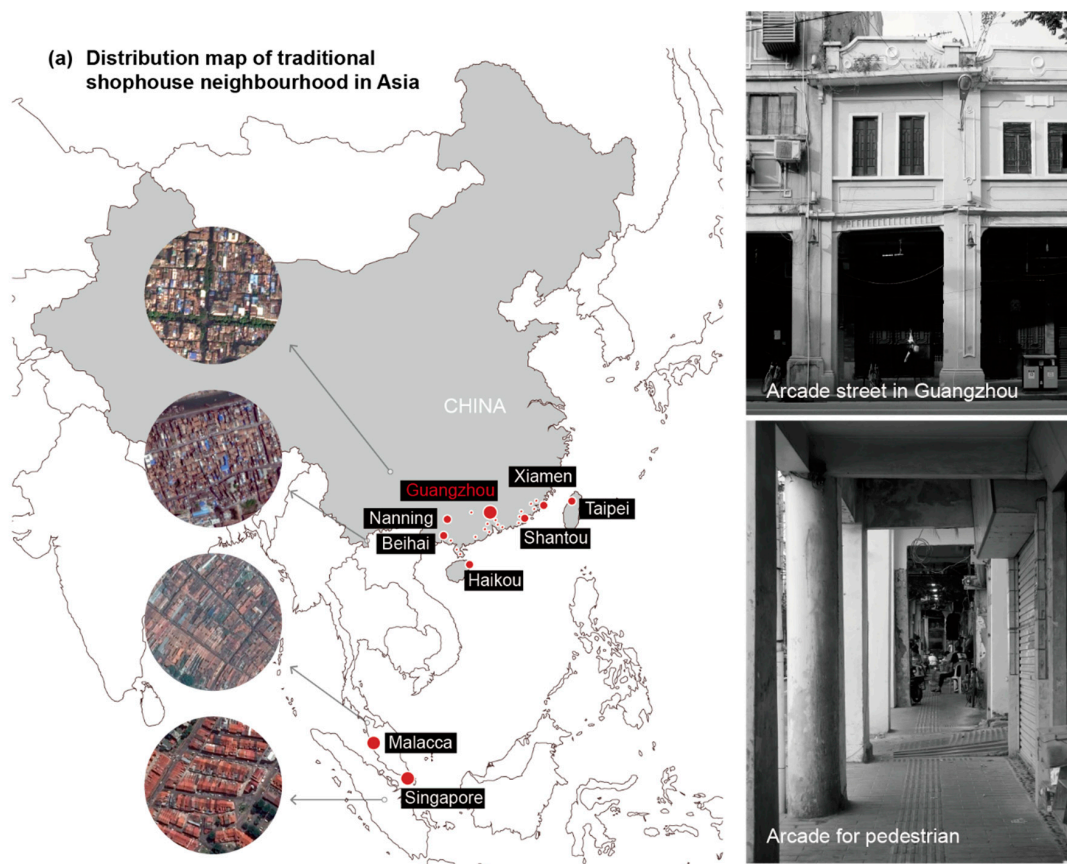


Figure 1. Cont.

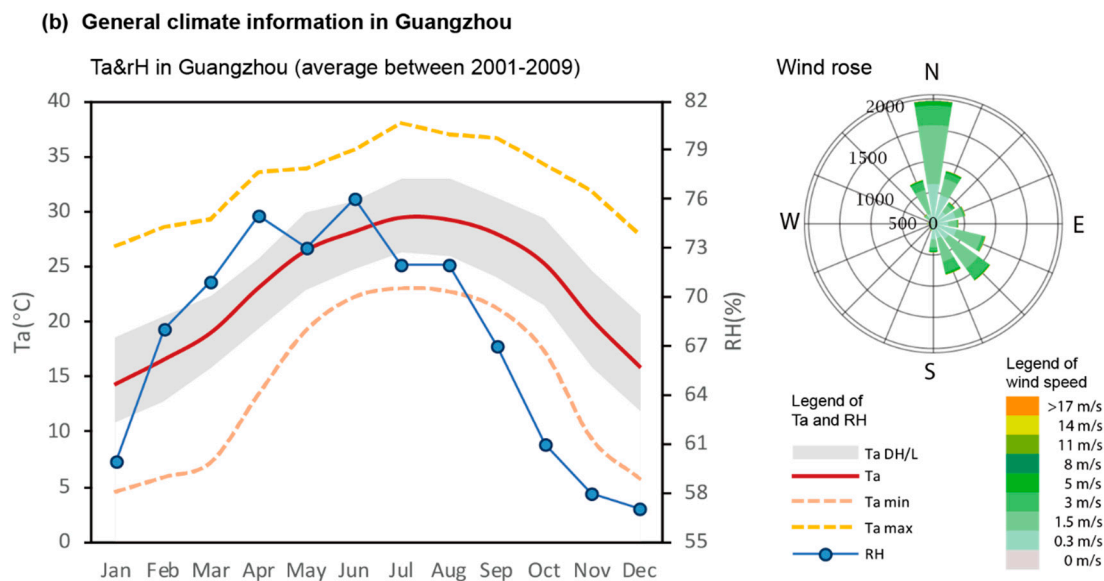


Figure 1. (a) The distribution of traditional shophouse neighbourhoods in southern China and southeast Asia. (b) The average air temperature and relative humidity in Guangzhou from 2001 to 2009; the wind rose with hours per year the wind blows from the indicated direction and wind speed. (Source: METEOTEST and Kunz [7]).

1.2. Literature

The impact of each variation from the basic configuration of a street canyon on the outdoor thermal environment has been studied intensely in recent decades. As reviewed in Jamei et al. [8], the impacts of street canyon design on pedestrian thermal comfort could be categorized into two groups: urban geometry and green infrastructure. The main variations in urban geometry include canyon aspect ratio (CHW) and orientation. There is no doubt that higher CHW values led to less radiation and better thermal comfort in the summer season [9–11]. Meanwhile, the street canyon orientation plays an important role in creating favourable environments for pedestrians, since it is associated with solar access [12] and wind flow [13]. The conclusions of these studies are similar: north-south (N-S)-oriented streets mitigate thermal stress in the summer, while east-west (E-W)-oriented streets suffer from heavier heat stress [14]. Green infrastructure is a highly recommended strategy for mitigating the urban heat island effect [15] and heat stress in street canyons [16] due to its valuable shadow and evapotranspiration effects [17]. In areas with similar climates, Morakinyo and Lam [18] reported the different effect among tree configuration parameters on outdoor thermal comfort, and the green streets showed less sensitivity to wind direction than streets without trees.

In addition to the impact of urban geometry and greenery, building-level shading strategies (e.g., arcade design), which are common in TSNs, are valuable in areas with hot climates [19,20]. In terms of the impact of arcades on outdoor thermal comfort, Ali-Toudert and Mayer [21] examined a deep street canyon and found that the physiological equivalent temperature (PET) in arcades was not as expected. The PET minimum (PETmin) in the arcade was same as that outside and PET maximum (PETmax) was 4 °C higher in the arcade than outside. Moreover, the relation between CHW and arcade on pedestrian thermal comfort in a single orientation was reported in previous research by the authors' former study [22]. However, the previous research on the impact of arcade on pedestrian thermal comfort is insufficient, such as the relation between aspect ratio of arcade with the solar access, and the correlation between arcade and other configurations in street canyon.

Despite the fruitful achievement of the previous studies, it is still difficult to use this knowledge to achieve transformation in practice [23]. As Erell [24] mentioned, urban planning and design is a complex process, requiring the designer to deal with a combination of parameters at multiple levels. Thus, from a holistic viewpoint, understanding the correlative impacts of design parameters on the

outdoor environment and their capacity for ameliorating thermal stress is helpful for designers dealing with geometric manipulation when balancing the outdoor thermal environment and other factors. The shading effect of buildings, umbrellas, and trees in an open area was compared by Lee et al. [25] in a warm summer continental climate (Dfb). The measurement results confirmed the building shading strategy presented a more effective cooling performance than the tree shading strategy, since it has a stronger ability to block shortwave radiation. Nevertheless, the research gap regarding the effect of the correlation between shading strategies and street configurations in canyon environments and thermal comfort still exists.

For predicting the impact of varying multi variations on outdoor thermal comfort, the microclimatic simulation software is used widely in current studies. For example, the computational fluid dynamics software performed well in simulating the pedestrian-level wind environment [26,27]; the CitySim Pro [28], SOLWEIG [29], Rayman model [30] and so on are contributing to predicting the impact of radiation fluxes on outdoor thermal comfort. The software applied in this study for simulating microclimate is ENVI-met (www.envi-met.com, science version V4.3, released in December 2017), since it is capable of performing the influence from all the variations, i.e., urban/building geometry and vegetation [31]. Meanwhile, a significant number of publications have reported the efficiency of the ENVI-met model in simulations of the outdoor environment [14,32–34].

2. Methods

To investigate the correlative impact of multiple design factors, a microclimatic measurement was first conducted in a TSN to compare the thermal performance of different types of street canyons and to validate corresponding simulation models. Then, a series of parametric models were simulated following the range of street scales from surveys by Yin and Xiao [22] on different canyons in TSNs.

2.1. Study Area and Monitoring

The study area was Guangzhou (23.1° N, 113.3° E), which is the largest city in southern China and has many TSNs in its old quarter, as shown in Figure 2a. The site was selected in the centre of old town and five pedestrian-level monitoring points (i.e., the point Al-s in an alley; Ar-w and Ar-e on the west and east sides of an arcade street; Tr-n and Tr-s in north and south sides of a boulevard, which is covered by a high density of *Flocculus banyan*) were used to record microclimatic variations. An additional point (approximately 15 m high) was set on a roof in this area as a weather station (WS). The specific locations and scale information of the measurement points are shown in Figure 2b,c. A fisheye photo was captured in the pedestrian area and central position of each monitoring street at a height of 1.5 m to measure their sky view factor (SVF). The SVF of WS is close to 0.90, which means that there is hardly any shading influence from other buildings or trees. It is obvious that arcade shading has greatly reduced the SVF relative to the other two canyons, whose values in the middle of the arcade are 0.053 and 0.103, respectively. However, the centre point of the street, Ar-m, is 0.442. Moreover, the high tree-covered area (TCA) (89%) in the boulevard canyon has the lowest SVF (0.165) in the middle of the street, but the SVF in the pedestrian area is still higher than that in the arcade, which is 0.062 in Tr-s.

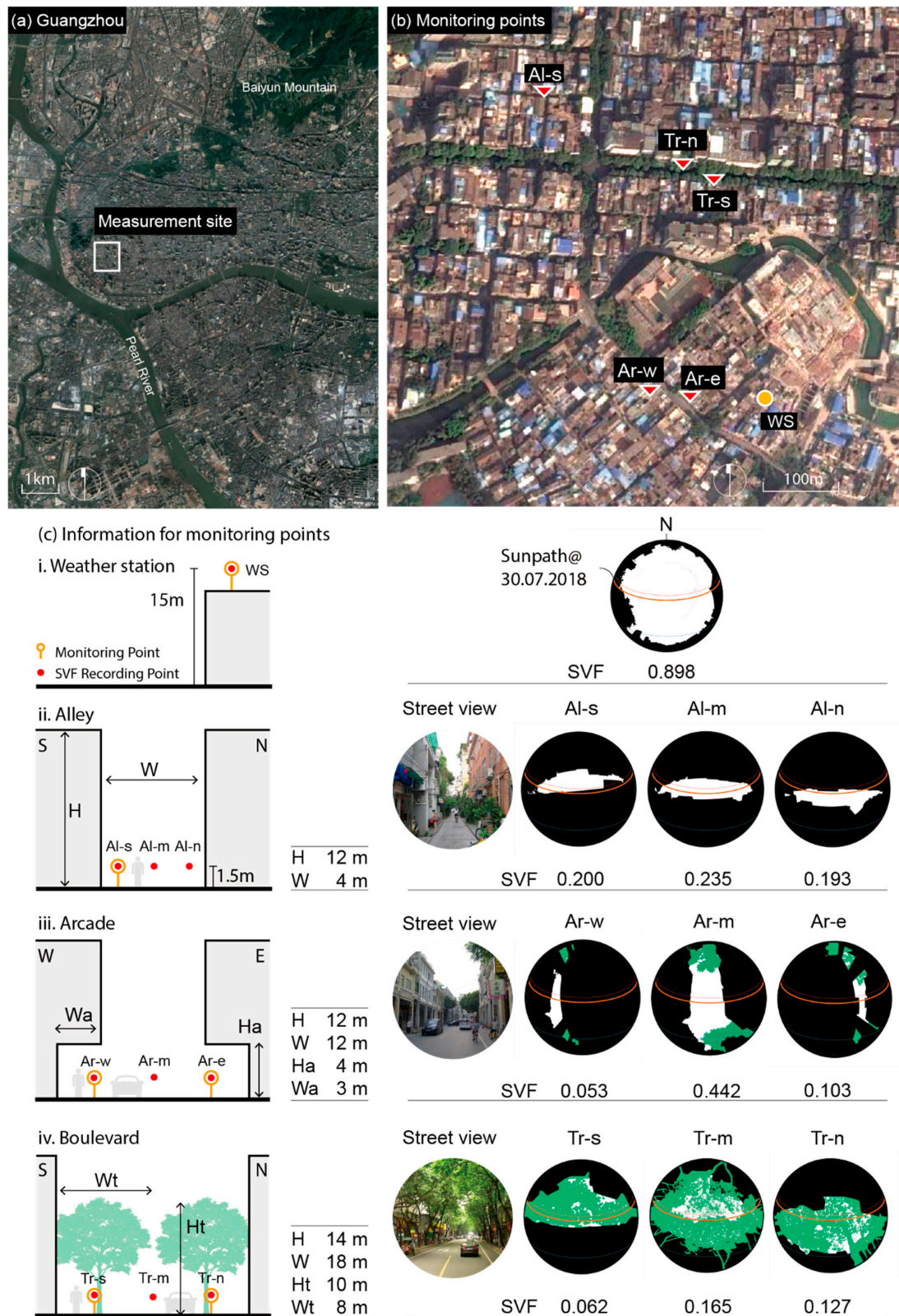


Figure 2. Study area and measurement points. (a) Location of the study area; (b) distribution of monitoring points; (c) street canyon and information of these points.

Monitoring took place on 30th July 2017, which is during the hottest period of the year. Table 1 lists the monitoring equipment for different points and the measured variables, which

include air temperature (T_a), relative humidity (RH), wind speed (V_a) and direction (W_{dir}), black global temperature (T_g), and global horizontal irradiation (GHI). Considering security problems, the monitoring time of pedestrian points was from 8:00 am to 8:00 pm local time, which coincides with the highest frequency of use of the urban public space. However, the WS point for recording regional weather data was measured for 24 h. The recording interval of all equipment was 5 min.

Table 1. Microclimate parameters and monitoring equipment.

Variable	Sensor Model	Accuracy	Resolution	Photo for Instruments
V_a	Delta OHM	HD 32.3/AP 3203.2	± 0.05 m/s	0.01 m/s
T_g		HD 32.3/TP 3276.2	class 1/3 DIN	0.1 °C
Radiation ²		DO 9847/LP PYRA 02	-	10 μ V/(W/m ²)
T_a and RH	Onset	HOBO Pro v2 U23-001 ¹	± 0.21 °C $\pm 2.5\%$	0.02 °C 0.03%
V_a and W_{dir} ²	Kestrel	NK 4500	± 0.1 m/s and $\pm 5^\circ$	0.1 m/s, 1°

¹ HOBO were set in Solar Radiation Shield. ² Measured only in the WS point.



2.2. Thermal Comfort Indices and Assessing Method

To assess pedestrian thermal comfort, the thermal comfort index was adopted as a comprehensive evaluation index in this research. Many thermal comfort indices derived from the human energy balance have been developed to evaluate the outdoor environment [35–39]. Among them, the physiological equivalent temperature (PET), developed by Höppe [38], was used as the thermal index for assessing pedestrian thermal comfort, since it considers both the meteorological environment and thermo-physiological parameters including the human energy balance. Moreover, PET is expressed in degrees Celsius (°C), which is user-friendly for both researchers and designers [14,32–34]. The human body model for PET calculation was based on a local investigation [40], which was a 35-year-old man, 1.75 m tall, weighs 75 kg, walking at a speed of 1.21 m/s, wearing clothes with an insulation factor of 0.3 m² K/W, and a sum metabolic work of 164.70 W/m². The *RayMan Pro* was used to calculate this index. As an indispensable variable when calculating the PET, the mean radiant temperature (MRT) of each monitoring point is calculated according to the following formula:

$$\text{MRT} = \left[(T_g + 273)^4 + \frac{1.1 \cdot 10^8 \cdot V_a^{0.6}}{\varepsilon \cdot D^{0.4}} \cdot (T_g - T_a) \right]^{0.25} - 273, \quad (1)$$

where D is global diameter (m) (0.038 m in this study), and ε is emissivity (0.95 for a black-coloured globe).

To further develop this assessment tool, PET is associated with the predicted mean vote index (PMV) proposed by Matzarakis and Mayer [41] to bridge the thermal perception and grade of physiological stress on human beings using the corresponding PET ranges for Western/middle Europeans, whose comfort range is defined as 18 to 23 °C and 20.5 °C for neutral PET, as residents in different climate zones have different tolerances to temperature and the ranges of thermal indices will vary as well [42]. According to many studies in hot and humid zones [43–45], the neutral PET in these areas is approximately 28 °C. This paper adopts the relation between PET and PMV examined by Lin and Matzarakis [43] for Taiwan, which has a climate zone that is similar to that of Guangzhou; the temperature range that produces no thermal stress is from 26 to 30 °C, which is much high than that in

Europe. Considering that, in this region, the PET is far beyond 42 °C in the summer season, the Extreme Heat Stress grade can be extended three more levels, ESH1 to ESH3, based on the correlation in the above study, as shown in Table 2, to evaluate the thermal environment more precisely.

Table 2. The extended version of the relation between physiological equivalent temperature (PET) range and the grade of physiological stress based on Lin and Matzarakis [43].

Thermal Perception	PET (°C)	Grade of Physiological Stress (PS)	Abbreviation
Very cold	<16	Extreme Cold Stress	ECS
Cold	16–18	Strong Cold	SC
Cool	18–22	Moderate Cold	MS
Slightly Cool	22–26	Slight Cold	SC
Comfort	26–30	No Thermal Stress	NTS
Slightly Warm	30–34	Slight Heat	SH
Warm	34–38	Moderate Heat	MH
Hot	38–42	Strong Heat	SH
Very Hot I	42–46	Extreme heat stress I	EHS1
Very Hot II	46–50	Extreme heat stress II	EHS2
Very Hot III	50–54	Extreme heat stress III	EHS3

As mentioned by Charalampopoulos et al. [46], the total thermal load could be taken into account to evaluate the outdoor thermal performance for a person in a certain period. Enlightened by this concept, the PET load (PETL, i.e., the part of PET over no thermal stress, as in the formula below) and the cumulative PETL (cPETL, i.e., the sum of PETL) were applied to assess the thermal stress load on the attendance of a person in a specific point [47]. In this research, the value of background condition (BC), which is 30 °C, was selected as the upper limit of NTS in Table 2.

$$\text{PETL} = \text{PET}_{\text{th}} - \text{BC}. \quad (2)$$

Here, PET_{th} is the average hourly PET value, and BC (background condition) in this section was set to denote the maximum PET for a PS grade of “no thermal stress” (i.e., a PET of 30 °C).

2.3. Simulation Studies

2.3.1. Software and Validation

To achieve desirable results, representative data from the actual site were needed as the boundary conditions in the simulation by ENVI-met. In this case, the monitoring data from the roof point (WS), including hourly T_a , RH, V_a , Wdir and global horizontal irradiation, were adopted in the forcing data file for the ENVI-met model.

Regarding the model for validation, three basic genetic models, for alley (AL), arcade street (AR), and boulevard (TR), respectively, were built for simulation according to the in-situ survey following the details in Figure 2. The buildings of the street canyon were simplified in a solid volume with a uniform height (H) and material composition, since those patios are too small to compare with the volume itself. The length of the street canyons (L) in all cases was 90 m so that they are all long canyons [48] whose L/H is over 7. The arcade part of AR has a 3-m depth and a 4-m height. The resolutions of grids are the divided equidistantly in X-, Y-, and Z-axis. The size of each grid was: $\Delta X = 1$ m, $\Delta Y = 1$ m, and $\Delta Z = 2$ m respectively. For increasing accuracy in calculating surface processes, the lowest grid cell above ground was split into five small cells with size of ΔZ . Thus, the height of lowest five grid cells were 0.4 m. The results from the receptor on the corresponding monitoring point at a height of 1.4 m (the midpoints of the fourth grid in Z-axis). Figure 3 indicates the simulation models for these basic canyons.

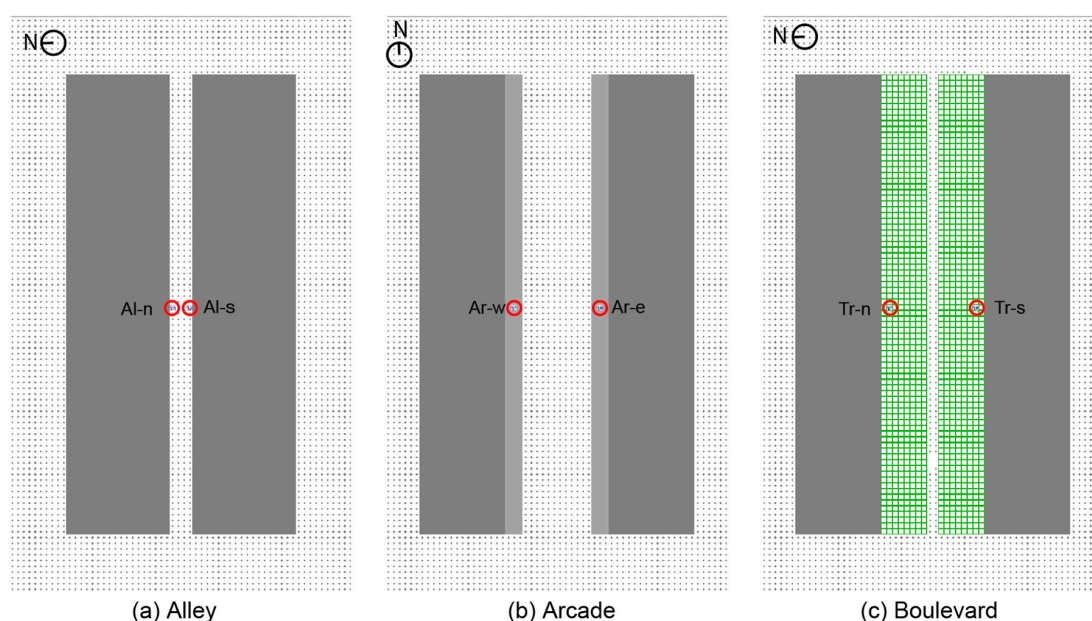


Figure 3. The simulation model for three different types of canyons and the positions of the receptors: (a) Alley, (b) Arcade street, (c) Boulevard.

Table 3 lists additional details about the boundary conditions for simulation. The street greenery in the TR canyon is *Flocculus banyan*, and the height of the trees is 12 m. The leaf area density (LAD) of tree model in ENVI-met (see Table 4) was built based on the situation in the field; the default settings (tree in very dense and free stem crown layer) and the value in other research [49,50].

Table 3. Climate data input for simulations with ENVI-met.

Variable	Settings
Size and resolution	100 × 100 × 50 m X = 1 m, Y = 1 m, Z = 2 m
Date	30.07.2017
Duration	4:00 am–8:00 pm
Initial T_a and RH	As monitoring data from WS point
Solar adjustment factor	0.78, max 847 W/m ²
Wind velocity and wind direction at 10 m	1.5 m/s, 135°
Specific humidity at 2500 m ¹	13.0 g/kg
Soil initial temperature ²	305 K (0–20 cm)/307 K (20–50 cm)/306 K (<50 cm)
Soil wetness ²	30% (0–20 cm)/40% (20–50 cm)/50% (<50 cm)
Building	Wall: Thermal resistance = 0.5 (m ² K)/W, albedo = 0.4 Roof: Thermal resistance = 1.0 (m ² K)/W, albedo = 0.45
Surface albedo	Asphalt = 0.2/Concrete = 0.8/Grey tile = 0.5

¹ This variable is acquired from <https://atmcorr.gsfc.nasa.gov>. ² This variable is acquired from Yang et al. [51].

Table 4. Leaf area density (LAD) profiles for trees in ENVI-met.

LAD (12 m)	LAD1	LAD2	LAD3	LAD4	LAD5	LAD6	LAD7	LAD8	LAD9	LAD10
	0.00	0.00	0.00	0.50	1.00	2.00	2.50	2.50	1.75	0.5

2.3.2. Parametrical Simulation Studies

Based on the boundary conditions for above basic models, five groups models were generated by varying corresponding parameters for examining the correlative relationship between shading strategy and street configuration. Specifically, as shown in Figure 4, Group 1 is an extended study on the alley,

in which the correlative impact from high CHW and canyon axis orientation on pedestrian thermal comfort is examined. Developed from the arcade street, Group 2-1 analyses the correlative impact of an arcade of a specific scale (same as it in validated model) with various CHW values and orientations on thermal comfort. As a further study, Group 2-2 is designed to discuss the impact of various arcade aspect ratios (AHWs) and orientations for a specific CHW ($H = 12$, $W = 12$). Group 3-1 examines the impact of various CHW values and orientations in a street canyon with a specific TCA value in the basic boulevard (TCA = 89%). Furthermore, Group 3-2 illustrates the effect of various TCA values by varying the radius of the vegetative crown ranges from 2 to 8 m (i.e., their TCAs from 22% to 89%) and orientations for the same CHW value with the basic boulevard ($H = 14$, $W = 18$).

As reported in a former study by authors on a scale survey of TSNs [22], the canyons with different shading strategy owned a corresponding range on CHW. The CHWs of alleys are always over 1, since their heights range from approximately 10 to 20 m and their widths vary between 2 and 9 m; street canyons with arcades are relative shallow, with a CHW value that is approximately equal to 1; and boulevards always have shallow canyons, with widths in the range from 15 to 25 m and heights of only 10 to 20 m. Moreover, the size of veranda in arcade street (relating the value of AHW) illustrates a small variance in terms of magnitude, with heights and widths of approximately 3 to 5 m. Based on above results, the range of CHW for the three canyon types can be defined as the following: from 1 to 3 in the AL (Group 1), from 0.75 to 2 in the AR (Group 2-1), and from 0.5 to 1.5 in the TR (Group 3-1). Moreover, AHW ranges from 0.8 to 2. Five cases were selected according to the above ranges with average intervals for each group, and the simulation models in ENVI-met were adjusted using only validated basic models by changing the building height. These generated models were named according to their group and the corresponding value of variable. To be specific, Group 1 to Group 3-2 is abbreviated as AL, AR, AC, TR, and TC respectively. The canyon with CHW in 3 in Group 1 is noted as AL300, and similarly TC089 alludes to the canyon with TCA in 89% in Group 3-2.

In the next step, these 25 cases were simulated in four different orientations, i.e., north-south (N-S), east-west (E-W), northwest-southeast (NW-SE), and northeast-southwest (NE-SW). In the end, a total of 100 street canyons were generated and simulated in ENVI-met under the same boundary conditions as those in validation (Table 3), except for the wind direction, which is always oblique to the corresponding orientation by 135° , and the midpoints on both sides of those pavements are targeted as the receptor for recording the microclimatic variations by hour. The data on the height of 1.4 m were used for the further analysis.

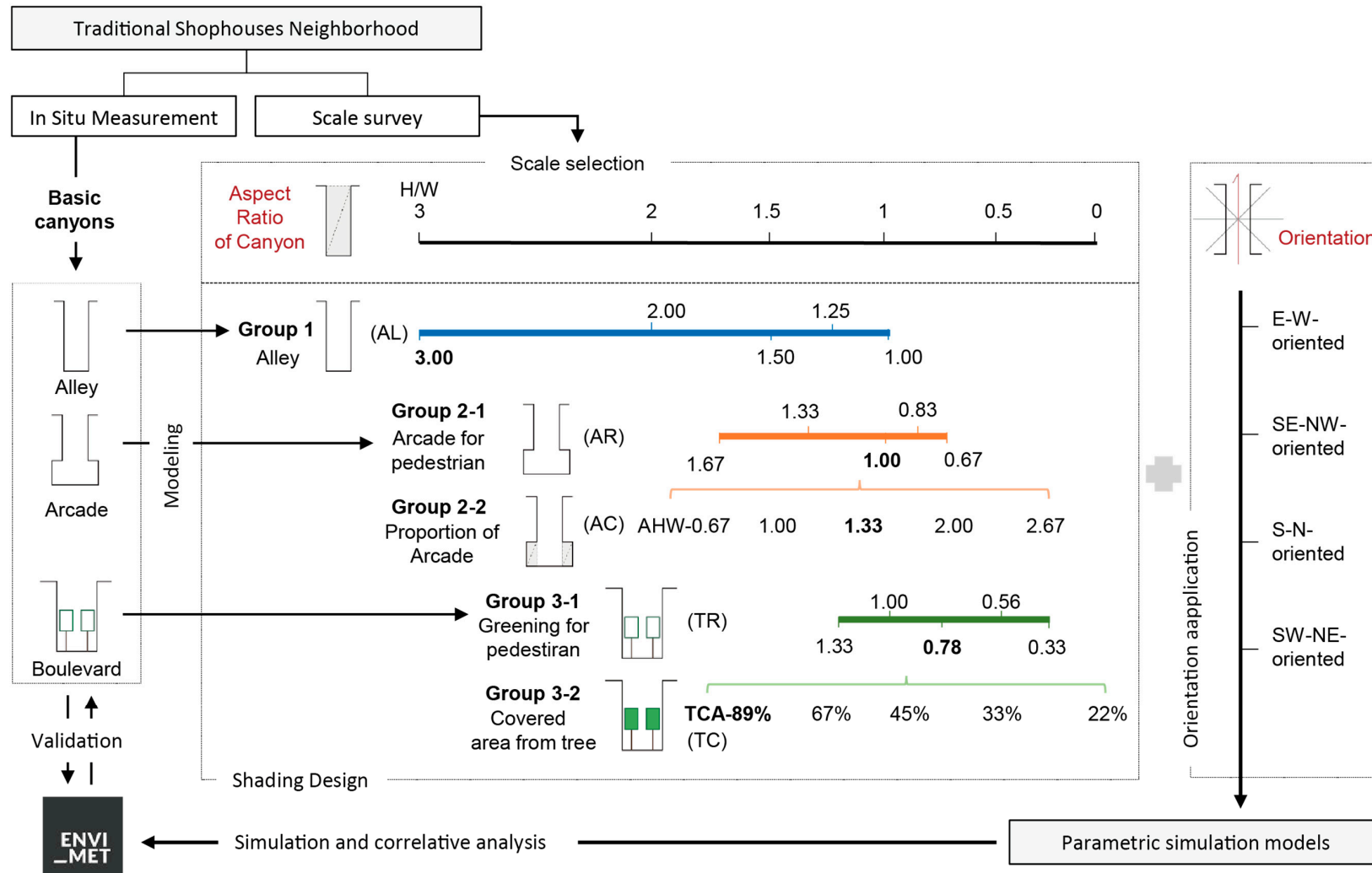


Figure 4. Schematic of the parametrical simulation for the correlative relationship between shading strategy and street configuration.

3. Results and Discussion

3.1. Measurement and Validation

Figure 5 indicates the local T_a and RH from the WS point on 30th July. To match the data for the forcing file in ENVI-met, all measured data were transferred to hourly measurements by calculating the average of 10 min before and after the hour. T_a reached its peak (38.7 °C) at 1600H and its minimum (27.1 °C) at 0200H, while the minimum of RH was 48.5% and its maximum of 90.1% was reached at 0700H. The solar adjustment factor of the ENVI-met model is set as 0.78 to fit the global horizontal irradiance from the measured point (WS), and the comparison result is shown in Figure 6.

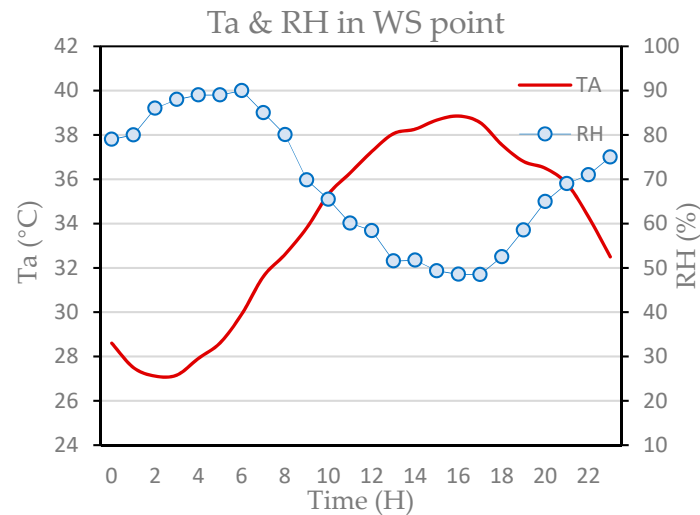


Figure 5. Hourly air temperature and relative humidity at WS on 30th July 2017.

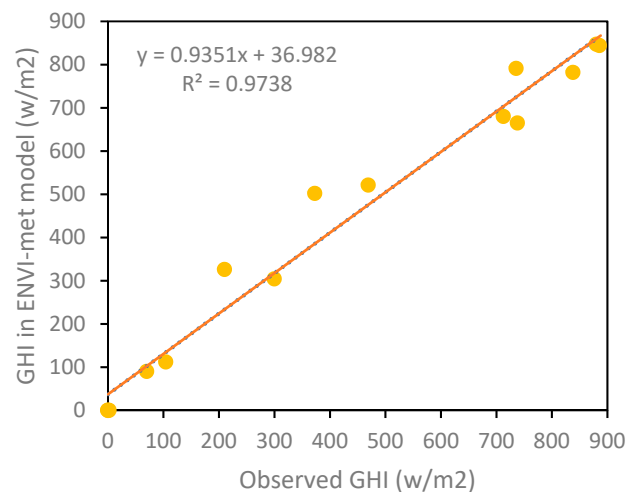


Figure 6. The scatterplot and regression line showing the relationship between observed global horizontal irradiance (GHI) at WS point on 30th July 2017 and in the ENVI-met model with a solar adjustment factor of 0.78 from 0600H to 2000H.

T_a , MRT, and PET are applied for the comparison between measurement and simulation (Figure 7). Regarding T_a , the results from ENVI-met present only a few differences between each other. The peaks of T_a from the simulated result are approximately 37 °C, while a discrepancy of approximately 1.5 °C exists between the measured points in the alley and the boulevard (i.e., O-Al-s and O-Tr-s) in peak time (38.7 and 36.9 °C at 1600H, respectively). This overestimation of T_a for canopy shading by trees in the ENVI-met simulation was also reported in Liu, Zheng and Zhao [50]. In contrast, the simulated values of MRT and PET illustrate distinct differences among the three canyons, and the PET value is

highly related to MRT. According to the result, the thermal stress for pedestrians was significantly ameliorated by high greenery coverage (PETmax was almost 10 °C less than that of the other street canyons). The point in the arcade could not avoid huge fluctuations in PET since it was out of the shade from the arcade in a certain period in the day (approximately 2 h for each point).

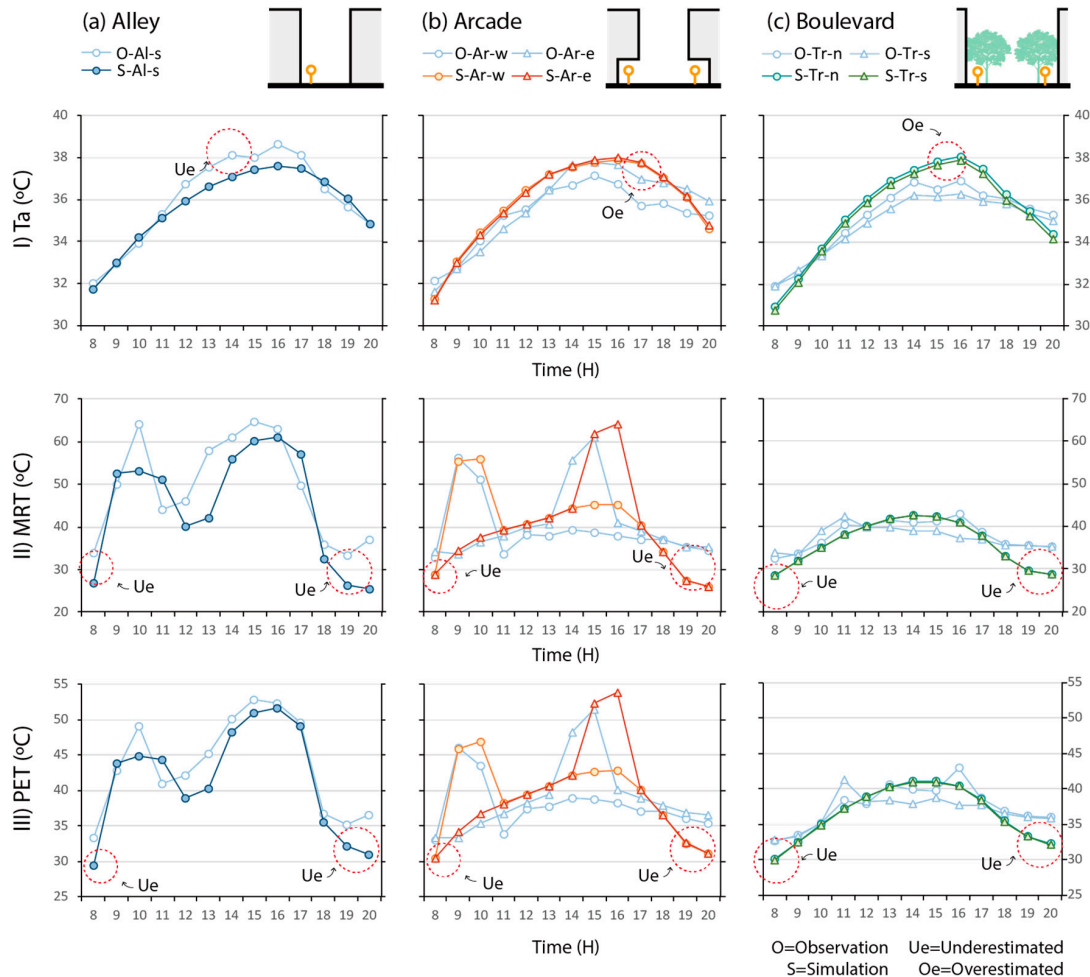


Figure 7. The comparison between the results from measurement and simulation in different street canyons: (a) Alley, (b) Arcade and (c) Boulevard.

However, it is worth noting that simulating MRT and PET results in severe underestimations at low radiation periods, e.g., 0800H, 1900H, and 2000H, in which the largest gap between the MRT values from observation and simulation (O-Al-s and S-Al-s) is more than 12.5 °C at 2000H. In addition to the beginning and ending times, the simulated PET values illustrate relative proficiency and smaller error compared to the result of MRT. For example, the maximum Δ MRT between the simulated and measured MRT values at 1000H in alley streets is 10.1 °C, while the maximum Δ PET is only 3.7 °C. Some peak times are not perfectly synchronous when simulating PET; for example, in arcade streets, PETmax is postponed 1 h, and in boulevard streets, the simulated PET does not fluctuate in the peak time, and measured PET is identical in all canyons.

Considering the above analysis, the simulated T_a from ENVI-met is not reliable between different canyons, and it is not suitable as an index for assessing the thermal environment. The monitoring and simulation of PET in different canyons presented relatively high coefficient in a certain period of time. Thus, only PET values in the daytime (from 0900H to 1800H) are used in the following analysis of parametric simulation.

3.2. Pedestrian Thermal Comfort in Parametrical Simulations

In this section, the results from all parametrical simulations are examined. The PET in each point is transformed and coloured to its corresponding thermal perception according to Table 2. A 2D compass coordinate system is applied in the following analysis for marking the corresponding points in different orientation canyons and the specific side of the pavement. The angle of the azimuth (θ) to the Y-axis in counter-clockwise, denoted as the θ of point (P θ) and referred to as the direction toward which the point faced to the road. For instance, the expressions “P0” and “P180” allude to the point in the north (0°) and south (180°) sides of the E-W-oriented streets, respectively. Thus, the eight points in four different orientations are indicated following the angle from 0° to 315° with an interval of 45°.

3.2.1. PET in Alleys (Group 1)

As shown in Figure 8a, the intensity and duration of EHS grade (PET >42 °C) in all points increased as the canyon became shallow. The pedestrians on the both sides of E-W-oriented alley suffered from the fiercest thermal stress, and the duration of EHS grade on the monitoring point was prolonged from 6 to 10 h in the E-W-oriented alley, with CHW varying from 1 to 3. In contrast, the points in the N-S-oriented alley showed the best thermal performance for pedestrians in all orientations, and the durations of the EHS grades in AL300 and AL100 were only 1 and 5 h, respectively. The other two orientations illustrated similar reactions with various CHW values, and the points on the west side, such as P45 and P135, had higher intensity of thermal stress than those on the east side. However, the duration over the EHS grade in the previous points was less than that in the eastern points (P225 and P315). Regarding PET, the pedestrians on both sides of the E-W-oriented alley had a peak time between 0900H and 1800H in all cases. Meanwhile, with CHW descending from 3 to 1, the increments of PETmax in P0 and P180 are inconspicuous (no more than 1 °C) according to Figure 8b. The peak values of other points are sensitive to CHW. For instance, PETmax in P45 raises 8.2 °C from AL300 to AL150; however, the values were insensitive in shallow canyons, i.e., only 0.9 °C from AL150 to AL100. However, in general, PETmax shows weak intensification and amplification in western points relative to that in eastern points. Figure 8c illustrates the symmetric characteristics of cumulative PETL in the east and west parts, even though PETmax on the east side was always higher than that on the west. There is a similar relation between aspect ratio and PETmax, with the increment of cPETL in P0 and P180 being relatively insensitive to CHW. For example, the cPETL in P0 increased only 23 °C from HW300 to HW100, while the cPETL in P90 increased 43.2 °C. P180, the point on the south side of street, illustrated the worst thermal environment, and cPETL of the point in the west side of the street was the highest in all cases.

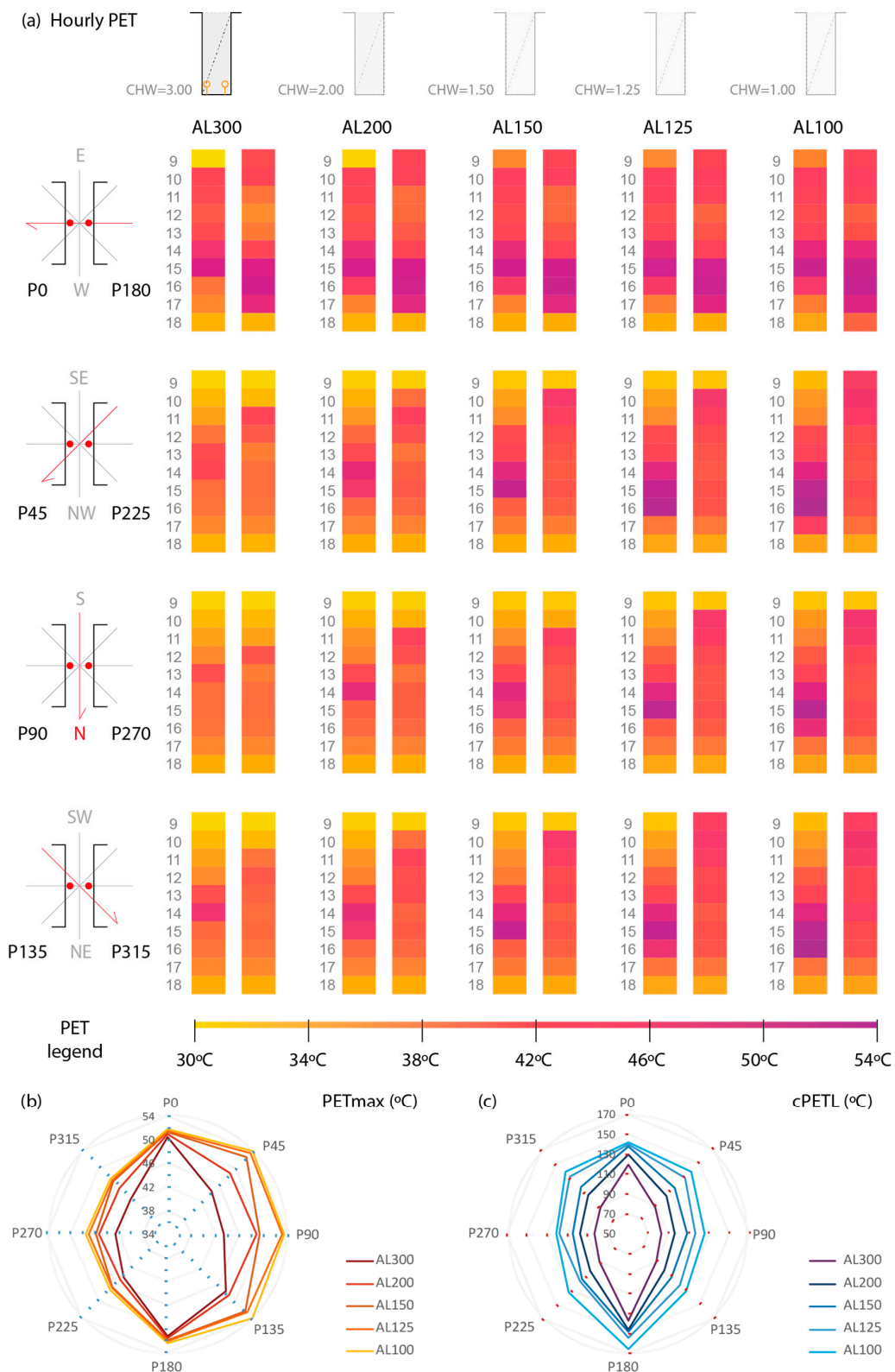


Figure 8. PET in alleys with varying aspect ratio of canyon and orientation. (a) Hourly grades of physiological stress (PS) based on PET in pedestrian points between 0900H to 1800H. (b) The maximum PET on 30th July 2017 between 0900H to 1800H. (c) The cumulative physiologically equivalent temperature loads (cPETL) for 30th July 2017 from 0900H to 1800H.

3.2.2. PET in Arcade Streets (Groups 2.1 and 2.2)

Comparing the PET in alleys, the duration over EHS grade in all points is significantly reduced by arcade shading (Figure 9a). For instance, only 3 h were over the EHS grade in the P90 with AR050, which was the worst thermal environment of all points in the arcade street. In contrast, the best thermal environment for pedestrians was in the E-W-oriented arcade streets (P0 and P180), in which there were hardly any periods over the EHS grade when varying the aspect ratio of the canyon. In the other streets, with CHW descending from 1.67 to 0.67, the duration of time spent over the EHS grade increases slowly, while only few increments of PET exist in other periods. As in the alleys, the eastern point performs worse in terms of ameliorating the thermal stress on pedestrians than the western point (e.g., peak PET in P45 is EHS3 at 1600H, but in P225, it is only EHS1 at 0900H). As shown in Figure 9b, only few changes exist in the PETmax of P0 and P180, but significant increases appeared in other points from HW167 to HW133. For AR167, the peak value (41.5 °C) was similar between different points, excluding P90, which is exposed to sunshine at 1500H, when PETmax reaches 52 °C. Regarding the cumulative PETL in arcade streets, as in PETmax, the points on the E-W-oriented arcade illustrated little sensitivity to the aspect ratio of the canyon (Figure 9c). Moreover, the sensitivity of points on the west side is different than that on the east side. Specifically, the cPETL of western points changed significantly only with CHW in the range from 1 to 1.67, while that of the eastern points varied over the whole range of CHW.

Figure 10 illustrates the further parametrical study to examine the correlation between AHW and orientation in CHW with 1. By varying AHW, the duration over EHS grade changed more significantly than that in Group 2.1. As shown in Figure 10a, the whole period is under the EHS grade in all points in AC067, while the duration over EHS grade in susceptible points, such as P45 to P315, increased to 3 or 4 h in AC267. Meanwhile, the shading effect from the arcade for P180 vanished in AHW267 at 1700H, and its PETmax raised to 42.2 °C according to Figure 10b. Moreover, the PETmax of all susceptible points reached an upper limit when AHW was over 1.33. As shown in Figure 10c, this phenomenon coincides with the impact on cPETL, since a relatively stable thermal environment in all points was controlled between 85 and 110 °C when AHW was less than 1.33. For example, the cPETL of P315 raised slowly from AC067 to AC133 (91.7 to 103.3 °C) and then increased dramatically to 123.0 °C in AC200.

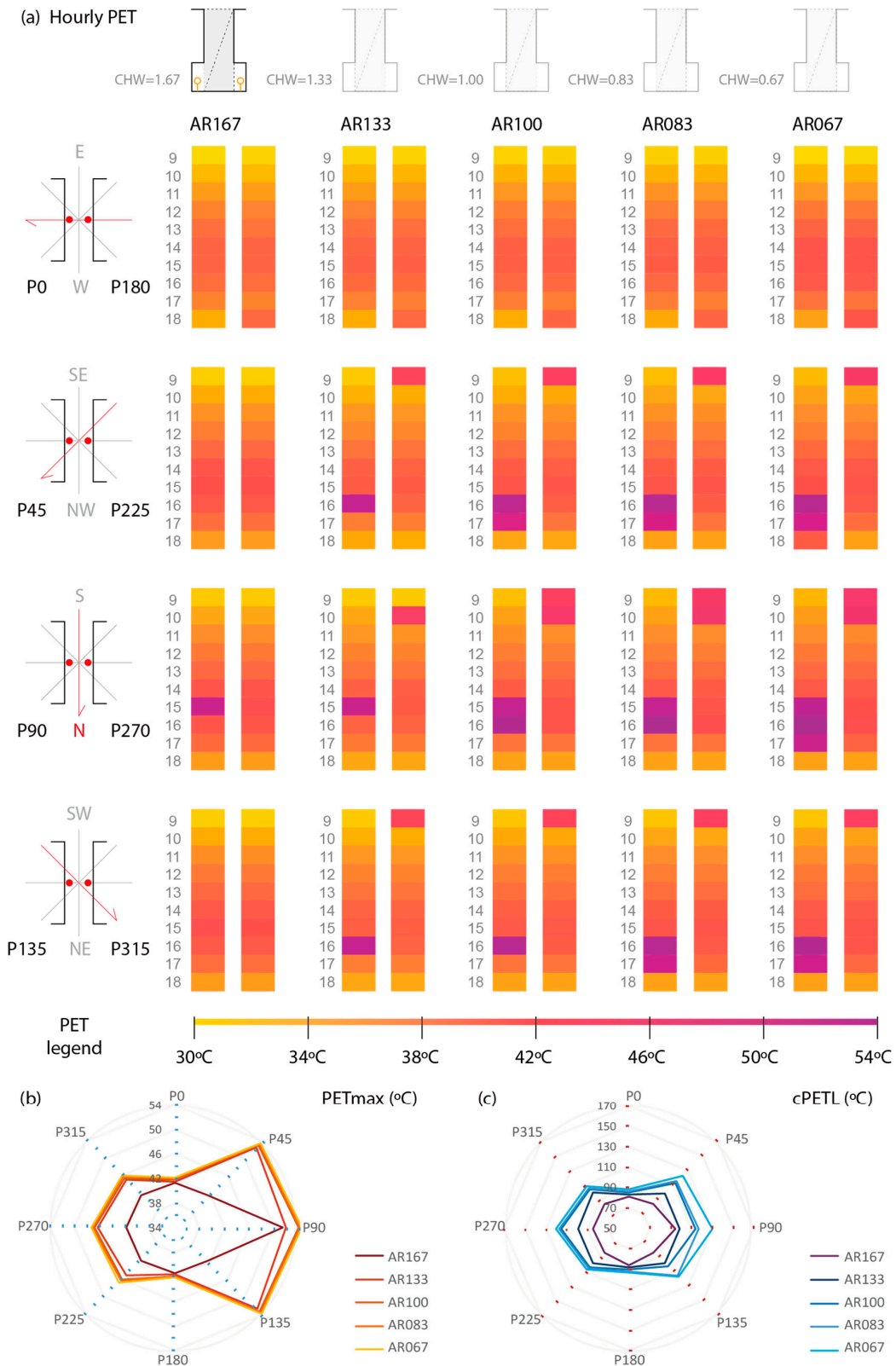


Figure 9. PET in arcades with specific proportions ($h = 4, w = 3$). (a) Hourly grades of physiological stress (PS) based on PET in all pedestrian points from 0900H to 1800H. (b) The maximum PET on 30th July 2017 from 0900H to 1800H. (c) The cumulative physiologically equivalent temperature load (cPETL) for 30th July 2017 from 0900H to 1800H.

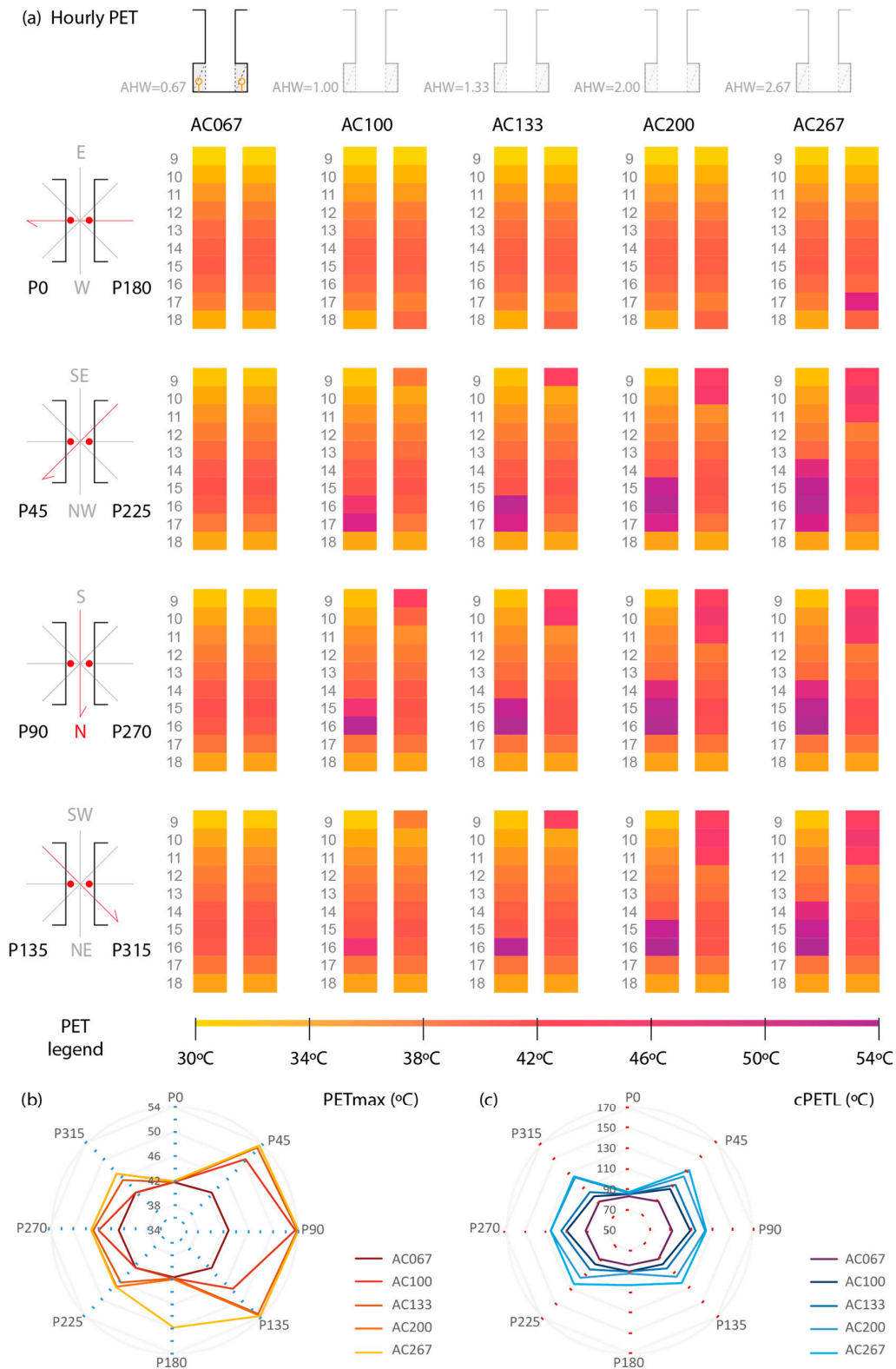


Figure 10. PET in arcades with varying proportions (AHW). (a) Hourly grades of physiological stress (PS) based on PET in all pedestrian points from 0900H to 1800H. (b) The maximum PET in 30th July 2017 from 0900H to 1800H. (c) The cumulative physiologically equivalent temperature load (cPETL) for 30th July 2017 from 0900H to 1800H.

3.2.3. PET in Boulevards (Groups 3.1 and 3.2)

As shown in Figure 11a, both CHW and orientation have a weak impact on the point on the street with dense greenery. By varying CHW from 0.78 to 1.33, the change of PET in all points is inconspicuous, and the whole period remains under the EHS grade. When the CHW is shallower than 0.78, the PET in all times increased in a relatively perceivable way, and the simulated points in all orientations are in the EHS1 grade in TR033 from 1400H to 1600H. Specifically, the PET of P90 at 1500H raised only 0.8 °C from TR133 to TR078, while from TR078 to TR033, this increment was 1.9 °C. Figure 11b illustrates that the PETmax values for different orientations in the same aspect ratio is similar, and the value increases relatively quickly when CHW is smaller than 0.78. For cPETL, a relatively weak impact existed on the cPETL of all points from TR133 to TR078, while a significant ascent occurred from TR078 to TR033, with Δ cPETL values of 7 and 16 °C, respectively, according to Figure 11c.

Figure 12 illustrates that the thermal environment of points on the east side rapidly deteriorated with decreasing tree-covered area (TCA), especially when TCA was less than 33%. As shown in Figure 12a, the PET of all points falls into the range from NTS grade to SH grade from TC089 to TC045. However, EHS grade occurred at susceptible points, P45 to P135, since the TCA was smaller than 33%; furthermore, a 2 h duration in EHS2 grade existed at these three points in TC022. As shown in Figure 12b, only the PETmax of points on the east side increased significantly when reducing TCA, with hardly any influence on points on the west side. For example, the reduction in TCA from 89% to 22% led to a promotion of 8.2 °C in P90, while it changed only 2.3 °C in point P270. Regarding cPETL, there are few impacts from varying TCA and orientation on pedestrian thermal comfort when TCA is over 33%, but there is a relatively huge increment in TC022 (excluding the point on the E-W-oriented street). According to Figure 12c, the streets with the highest cPETL, which is over 109 °C in TC022 canyon, are in P45, P90 and P270.

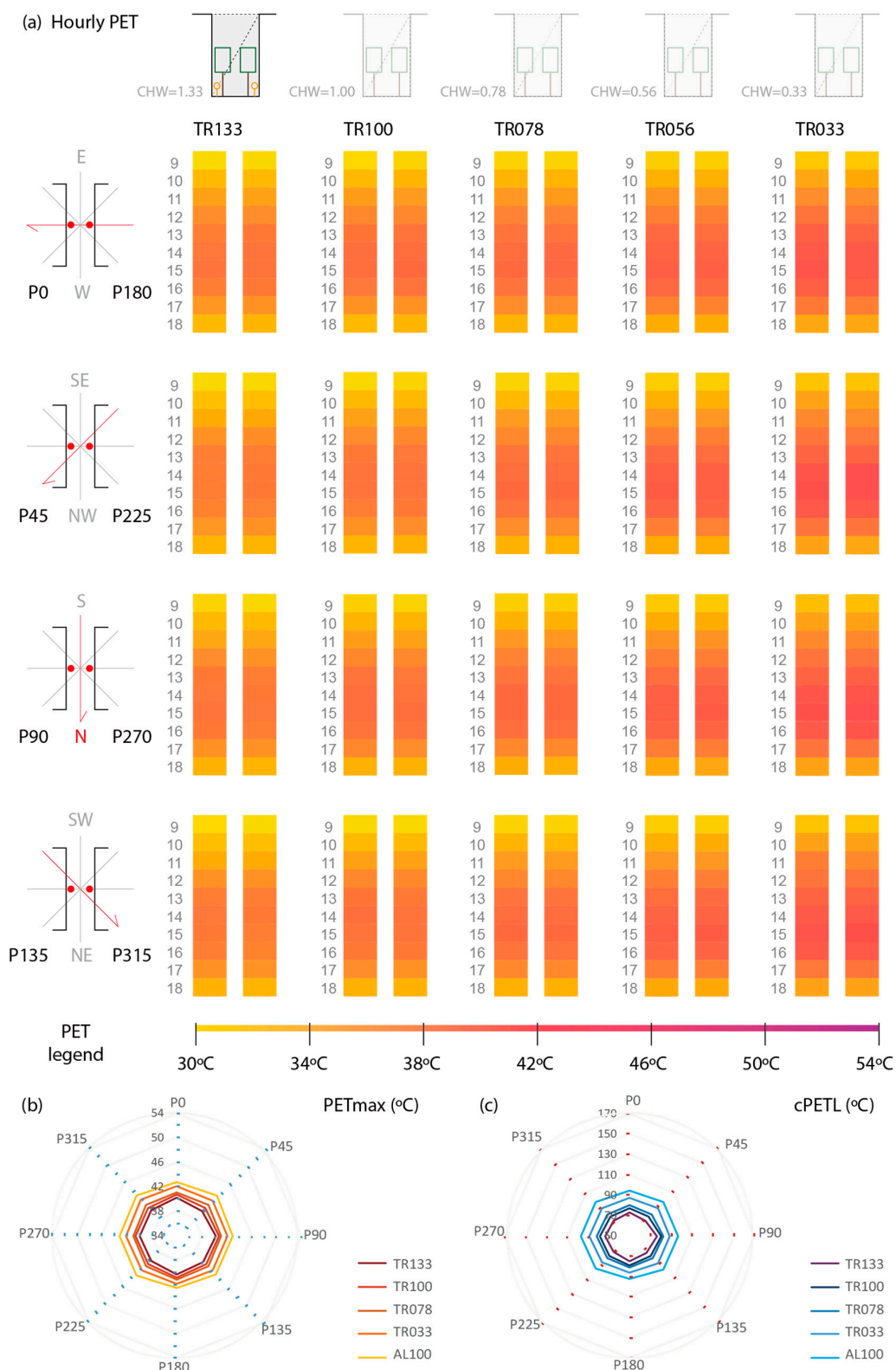


Figure 11. PET in boulevards with a specific tree-covered area of 89%. (a) Hourly grades of physiological stress (PS) based on PET in all pedestrian points from 0900H to 1800H. (b) The maximum PET on 30th July 2017 from 0900H to 1800H. (c) The cumulative physiologically equivalent temperature load (cPETL) for 30th July 2017 from 0900H to 1800H.

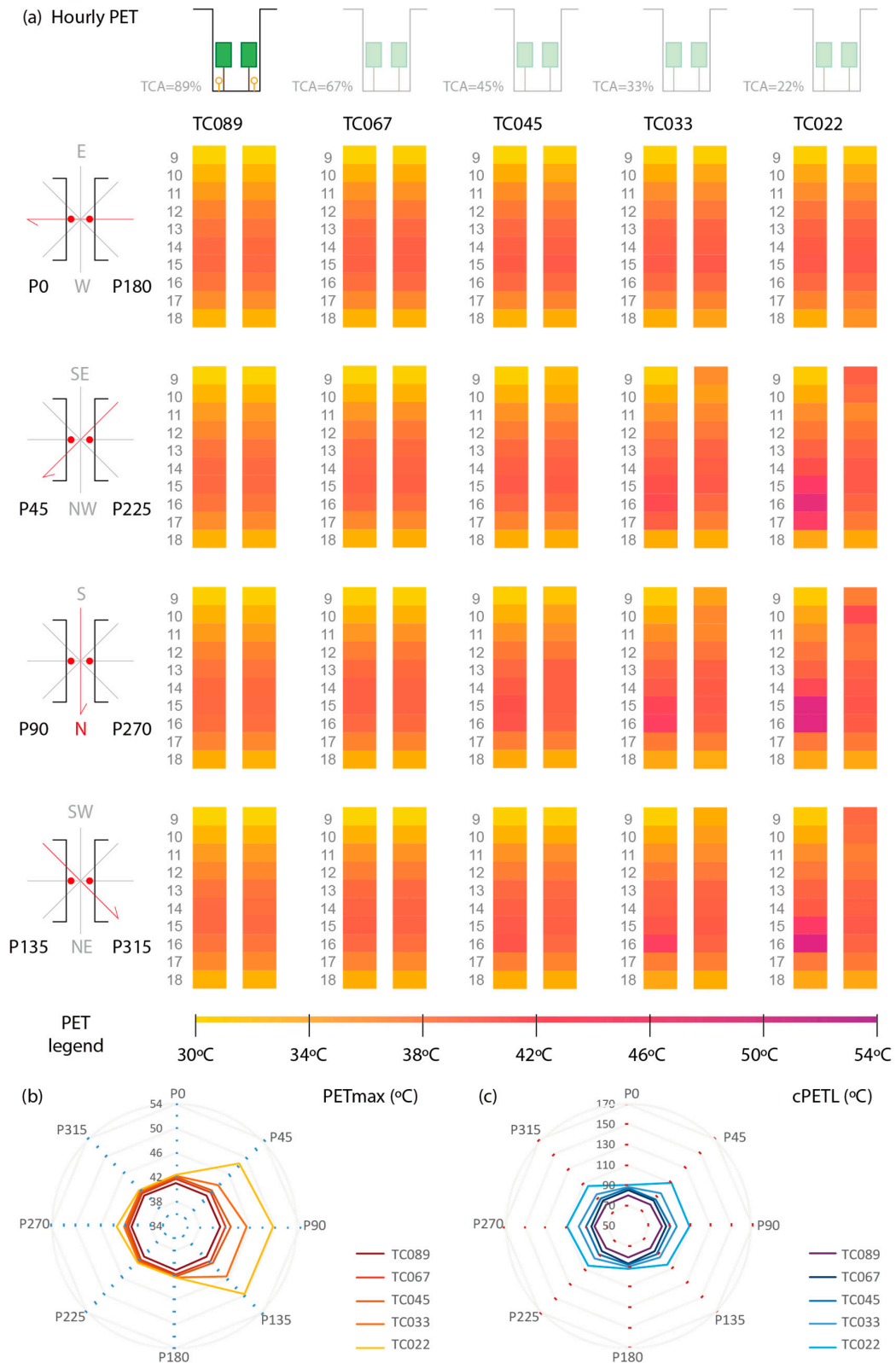


Figure 12. PET in boulevards with varying tree-covered area (TCA). (a) Hourly grades of physiological stress (PS) based on PET in all pedestrian points from 0900H to 1800H. (b) The maximum PET on 30th July 2017 from 0900H to 1800H. (c) The cumulative physiologically equivalent temperature load (cPETL) for 30th July 2017 from 0900H to 1800H.

3.3. Correlation between Multiple Design Factors and cPETL

Figure 13 illustrates the cPETL of all points from the parametrical simulation. In general, when comparing the result from Groups 1 (AL), 2-1 (AR) and 3-1 (TR), the cPETL of the points in boulevard streets are lower than those in other street canyons in any orientation; conversely, those in alleys are always highest. The gaps between the cPETL in AL and TR with the same CHW is always maintained at least 40 °C, and the maximum of these gaps reached over 80 °C comparing the P180 in AL with points in TR. According to the trendline of points in different orientations, the changes of Group TR are similar. In contrast, a significant difference exists between points of Groups AL and AR in varying orientations in terms of responding to the change of the aspect ratio of the canyon. Apart from these above special points in AL and AR, an inflection point appears in each group in varying CHW. The inflection for most points in AL and the all points in TR is the CHW with 1.5 and 0.78 respectively, since the growth ratio of cPETL accelerated with CHW smaller than that value. The P0 in AL presented a relative steady increase on cPETL as its CHW descended from 3 to 1. The situation in Group AR is more complicated: firstly, the P0 in AR illustrated a similar tendency with the P0 in AL whose growth of cPETL is the flattest, and its cPETL is forecasted as the same as or even lower than those in some point in TR, when the CHW lower 0.5; Moreover, a different inflection point exists in varying orientations and the tendency of these points is conversely comparing those in AL and TR. The cPETL of P315 and P225 in AR start to slow down the growth after their CHW is lower 1.33. Such inflection in other points is 1. Regarding the cPETL from Group 2-2 (AC), the points in AC200 and AC267 have already the same high cPETL as the points in the alley. For Group 3-3 (TC), the cPETL in the lowest coverage area is similar to those in P315 and P225 of the arcade street but still much lower than the other points in the arcade (except the P0 in AR).

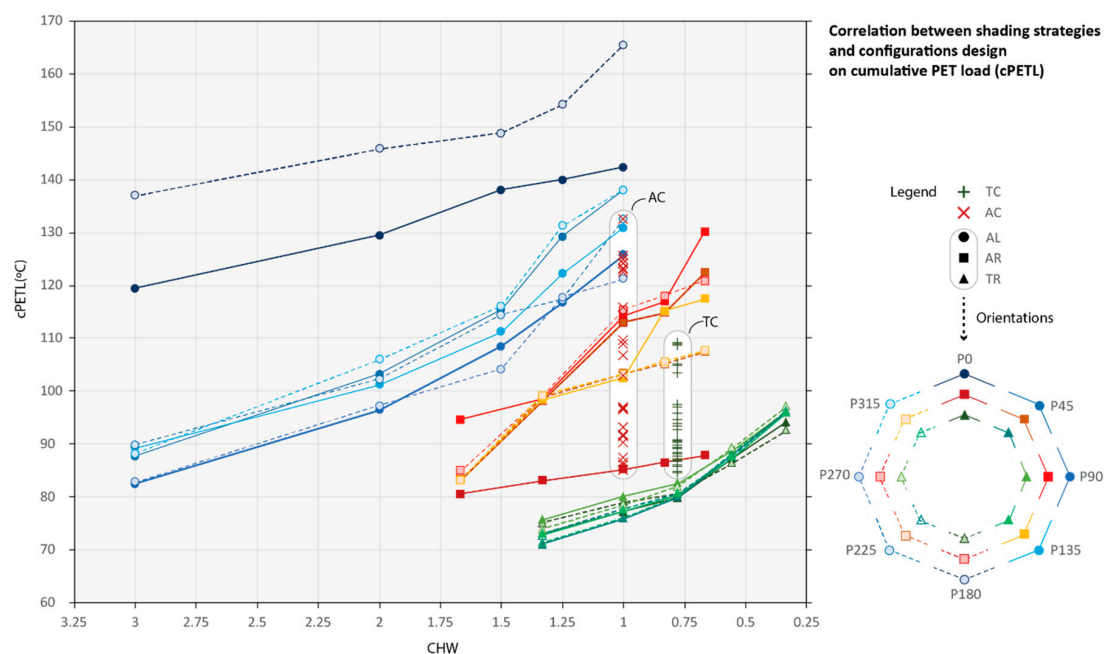


Figure 13. Comparison of cPETL from different parametrical simulations.

4. Discussion

The results of the microclimatic measurement illustrate the features of the thermal environment of canyons with different pedestrian shading strategies. Among these strategies, arcade shading with SE-NW orientation could not avoid direct exposure to solar beams during the daytime, and pedestrians suffered extreme thermal stress at certain times. However, the duration of extreme thermal stress was shortened compared to points in the E-W-oriented alley, although the intensity was the same. The only location where no obvious fluctuations in PET appeared was the point under the high-density

tree canopy, as the sun path was hiding in the tree canopy area at all times for this E-W-oriented boulevard, according to the SVF in Figure 2c. For the other periods without fluctuations, MRT and PET were similar.

Further parametric simulations investigated five groups with different design factors, including orientation, CHW, AHW, and TCA, based on the scale data from TSN. The correlations among them were revealed after analysing the results:

- At first, Group 1 was used to examine the impact of high CHW without extra shading on optimizing pedestrian thermal comfort. According to the results, the axis orientation of the canyon played an essential role on the effectiveness of ameliorating the thermal stress for pedestrians by increasing CHW. As many studies reported [10,14,52], E-W-oriented alley always provided worse thermal comfort for pedestrians than alleys with other orientations, and they were less responsive to CHW. In contrast, the N-S orientation performs best among these orientations, and the cPETL of other points in non-E-W-oriented alleys declined as their canyon deepened. However, this research finds out that the CHW in 1.5 is the inflection point for alleys, except E-W-oriented one, in this climate zone. A relatively large growth appeared in cPETL at these points in which the CHW was shallower than 1.5.
- The shading from the arcade had a totally different response to the axis orientation of the canyon than the shading in alleys, since better thermal conditions for pedestrians occurred in E-W-oriented streets with arcades. The cPETL of P0 in AR067 was almost the same as that of the points in the boulevard with high TCA and even better than that in lower TCA. The result coincides with other previous research on reporting better effectiveness of shading from buildings [25]. However, the arcade failed to avoid the discomfort at peak times of T_a in N-S-oriented streets with arcades, which is supported by the results of Ali-Toudert and Mayer [21]. Apart from P0, the other points in arcade street have their own inflection point in varying CHW, such as P315 and P225, which have values of 1.33. The point for other cases is 1. The cPETL of pedestrians reduced prominently when CHW was over the inflection point. Regarding the impact of AHW in the specific CHW with 1, PETmax decreased only when AHW was lower than 1.33, and a uniform thermal environment was achieved only in AHW067. Moreover, the thermal environment of P180, on the south side, started to deteriorate for AHW over 2.
- Unlike the former, orientation has hardly any impact on pedestrian thermal comfort for streets with high greenery coverage (TC089, Group 3-1). However, the impact of orientation intensified with decreasing on tree coverage area and was related to planting pattern and tree species [18,53]. Meanwhile, the cPETL of all points on the pavement from Group 3-1 increased faster when CHW was lower than 0.78. Regarding the impact of TCA (Group 3-2), pedestrian thermal comfort deteriorated significantly when TCA was lower than 33% in the canyon with CHW in 078, except for the points in the E-W-oriented boulevard.

After the above discussion, the mechanism of climate adaptation in TSN was also reintroduced. The canyons of TSN integrated shading and applied proper variables of street configuration to achieve a desirable environment for pedestrians. The above results could be served as a set of guidelines for non-climatic designers at early phases of urban design or planning. By means of these principles, the thermal conditions in street canyons would be predicted and optimized by selecting appropriate measurements and street configurations. For example, the E-W-oriented street with arcade and greening design ameliorates thermal stress for pedestrians prominently. Furthermore, the fluctuation in N-S-oriented streets can be avoided by applying arcade and greening in proper AHW and TCA respectively.

Last but not least, the main purpose of this study is to offer practical guidelines for ameliorating thermal stress from a design perspective rather than the issue of urban heat island. Thus, this research only focused on pedestrian thermal comfort rather than the thermal environment in the whole

canyon area. Some essential variables of pedestrian thermal comfort, such as the impact of SVF [32], the wind environment [54], the species of tree [18,55], the material composition of the building and pavement [56] and the asymmetry of the canyon [21,57], are rarely mentioned in this research. The studied parameters in this paper are convenient for adjusting, relating to the urban perspective directly, and more familiar and practical at early design stages. The other variations missing in this research are essential for urban climate without any doubt. The further study with a more overall view on the correlative impact among them is needed in the future. Some limitations from ENVI-met also have to be mentioned here, as they will affect the accuracy of predicting the wind environment [58] and estimating MRT in low-radiation flux periods [51,59,60]. Even though representative data from the actual site were adapted in this research, simulation errors are still difficult to avoid, since only the hourly air temperature and relative humidity can be imputed as boundary conditions.

5. Conclusions

This study, which investigated the impact of different shading strategies in street canyons on pedestrian thermal comfort, was inspired by the traditional shophouse neighbourhoods in southern China. Using field measurements and parametric simulations with scale data from local neighbourhoods, climate adaptation was revealed by correlating these shading strategies with basic street configurations. The findings are summarized in follows:

- (a) In general, the outdoor thermal comfort for pedestrian in alleys without any shading strategy are always worse than the other two street canyons in the same CHW of alleys. The shading from greenery illustrates the highest effectiveness on ameliorating the thermal stress of pedestrians.
- (b) The orientation only displays a significant contribution on pedestrian thermal comfort in alleys and arcade streets. Specifically, the E-W-oriented alleys always provide worse thermal comfort for pedestrians than the other orientations, and the pavement is better shaded on streets in the N-S orientation. However, the response on varying orientation is totally reversed in arcade streets compared to alleys and boulevards. The deep arcades feature a relatively uniform thermal environment in all orientations.
- (c) Regarding the influence of CHW, apart from some insensitive orientations, the trend of thermal environment in alleys towards rapid deterioration when its CHW is lower than 1.5. Such similar fluctuation for all boulevards (TCA = 89%) is 0.75. In contrast, the cPETL in arcades closely relates to CHW only when the latter higher than 1.
- (d) The shading for pedestrian from arcades (CHW = 1) becomes weak in AHW higher than 1.33, but these arcades still function well for the point in north side of E-W-oriented arcade. The points in the east side of boulevard (CHW = 0.78) starts losing shading from greenery when the TCA is lower than 33%.

The above results provide a valuable guideline for urban design in terms of optimizing the thermal environment of pedestrians by adopting a shading strategy that corresponds to the street canyon.

Author Contributions: S.Y. organized the paper, conducted experiments, wrote most of the text, and prepared all figures. W.L. and Y.X. provided valuable ideas, guidance with the methodology, research funding and facilities. Z.X. helped in data analysis and reviewing.

Funding: This work was jointly supported by the National Natural Science Foundation of China [No. 51478188 and 51138004] and the State Key Laboratory of Subtropical Building Science, South China University of Technology, China [No. 2014ZC08].

Acknowledgments: The authors would like to thank the Institute of Energy Efficient and Sustainable Design and Building (ENPB) of the Technical University of Munich (TUM) and our colleagues at the Centre for Urban Ecology and Climate Adaptation (ZSK) for providing abundant guidance and support on methods and techniques.

Conflicts of Interest: The authors declare no conflict of interest.

References

1. Lu Luber, G.; McGeehin, M. Climate change and extreme heat events. *Am. J. Prev. Med.* **2008**, *35*, 429–435. [[CrossRef](#)] [[PubMed](#)]
2. Raven, J. Cooling the public realm: Climate-resilient urban design. In *Resilient Cities*; Springer: Berlin, Germany, 2011; pp. 451–463.
3. Piesik, S. *HABITAT—Vernacular Architecture for a Changing Planet*, 1st ed.; DETAIL: Munich, Germany, 2017.
4. Han, W.; Beisi, J. A Morphological Study of Traditional Shophouse in China and Southeast Asia. *Procedia Soc. Behav. Sci.* **2015**, *179*, 237–249. [[CrossRef](#)]
5. Yeang, K. *The Architecture of Malaysia*; Pepin Press: Amsterdam, The Netherlands, 1992.
6. Lee, H.Y. The Singapore shophouse: An Anglo-Chinese urban vernacular. In *Asia's Old Dwellings: Tradition, Resilience, and Change*; Oxford University Press: New York, NY, USA, 2002; pp. 115–134.
7. Meteotest, J.R.; Kunz, S. *Meteonorm Data (Worldwide)*; METEOTEST: Bern, Switzerland, 2017.
8. Jamei, E.; Rajagopalan, P.; Seyedmahmoudian, M.; Jamei, Y. Review on the impact of urban geometry and pedestrian level greening on outdoor thermal comfort. *Renew. Sustain. Energy Rev.* **2016**, *54*, 1002–1017. [[CrossRef](#)]
9. Oke, T.R. Street design and urban canopy layer climate. *Energy Build.* **1988**, *11*, 103–113. [[CrossRef](#)]
10. Pearlmutter, D.; Berliner, P.; Shaviv, E. Integrated modeling of pedestrian energy exchange and thermal comfort in urban street canyons. *Build. Environ.* **2007**, *42*, 2396–2409. [[CrossRef](#)]
11. Jihad, A.S.; Tahiri, M. Modeling the urban geometry influence on outdoor thermal comfort in the case of Moroccan microclimate. *Urban Clim.* **2016**, *16*, 25–42. [[CrossRef](#)]
12. Herrmann, J.; Matzarakis, A. Mean radiant temperature in idealised urban canyons—Examples from Freiburg, Germany. *Int. J. Biometeorol.* **2012**, *56*, 199–203. [[CrossRef](#)] [[PubMed](#)]
13. Yang, F.; Qian, F.; Lau, S.S. Urban form and density as indicators for summertime outdoor ventilation potential: A case study on high-rise housing in Shanghai. *Build. Environ.* **2013**, *70*, 122–137. [[CrossRef](#)]
14. Ali-Toudert, F.; Mayer, H. Numerical study on the effects of aspect ratio and orientation of an urban street canyon on outdoor thermal comfort in hot and dry climate. *Build. Environ.* **2006**, *41*, 94–108. [[CrossRef](#)]
15. Tan, Z.; Lau, K.K.-L.; Ng, E. Urban tree design approaches for mitigating daytime urban heat island effects in a high-density urban environment. *Energy Build.* **2016**, *114*, 265–274. [[CrossRef](#)]
16. Zölch, T.; Maderspacher, J.; Wamsler, C.; Pauleit, S. Using green infrastructure for urban climate-proofing: An evaluation of heat mitigation measures at the micro-scale. *Urban For. Urban Green.* **2016**, *20*, 305–316. [[CrossRef](#)]
17. Perini, K.; Magliocco, A. Effects of vegetation, urban density, building height, and atmospheric conditions on local temperatures and thermal comfort. *Urban For. Urban Green.* **2014**, *13*, 495–506. [[CrossRef](#)]
18. Morakinyo, T.E.; Lam, Y.F. Simulation study on the impact of tree-configuration, planting pattern and wind condition on street-canyon's micro-climate and thermal comfort. *Build. Environ.* **2016**, *103*, 262–275. [[CrossRef](#)]
19. Mazouz, S.; Zerouala, M.S. Shading as a modulator for the design of urban layouts based on vernacular experiences. *Energy Build.* **1998**, *29*, 11–15. [[CrossRef](#)]
20. Lechner, N. *Heating, Cooling, Lighting: Sustainable Design Methods for Architects*; John Wiley & Sons: Hoboken, NJ, USA, 2014.
21. Ali-Toudert, F.; Mayer, H. Effects of asymmetry, galleries, overhanging façades and vegetation on thermal comfort in urban street canyons. *Sol. Energy* **2007**, *81*, 742–754. [[CrossRef](#)]
22. Yin, S.; Xiao, Y. Scale Study of Traditional Shophouse Street in South of China Based on Outdoor Thermal Comfort. *Procedia Eng.* **2016**, *169*, 232–239. [[CrossRef](#)]
23. Eliasson, I. The use of climate knowledge in urban planning. *Landsc. Urban Plan.* **2000**, *48*, 31–44. [[CrossRef](#)]
24. Erell, E. The Application of Urban Climate Research in the Design of Cities. *Adv. Build. Energy Res.* **2008**, *2*, 95–121. [[CrossRef](#)]
25. Lee, I.; Voogt, J.A.; Gillespie, T.J. Analysis and Comparison of Shading Strategies to Increase Human Thermal Comfort in Urban Areas. *Atmosphere* **2018**, *9*, 91. [[CrossRef](#)]
26. Liu, J.; Niu, J. Delayed detached eddy simulation of pedestrian-level wind around a building array—The potential to save computing resources. *Build. Environ.* **2019**, *152*, 28–38. [[CrossRef](#)]

27. Liu, J.; Niu, J.; Du, Y.; Mak, C.M.; Zhang, Y. LES for pedestrian level wind around an idealized building array—Assessment of sensitivity to influencing parameters. *Sustain. Cities Soc.* **2019**, *44*, 406–415. [CrossRef]
28. Walter, E.; Kämpf, J.H. A verification of CitySim results using the BESTEST and monitored consumption values. In Proceedings of the 2nd Building Simulation Applications Conference, Bozen-Bolzano, Italy, 4–6 February 2015.
29. Lindberg, F.; Thorsson, S. SOLWEIG—the new model for calculating the mean radiant temperature. In Proceedings of the Seventh International Conference on Urban Climate, Yokohama, Japan, 29 June–3 July 2009.
30. Matzarakis, A.; Rutz, F.; Mayer, H. Modelling radiation fluxes in simple and complex environments—Application of the RayMan model. *Int. J. Biometeorol.* **2007**, *51*, 323–334. [CrossRef] [PubMed]
31. Bruse, M. ENVI-met 4. A Holistic Microclimate Modelling System. Available online: <http://www.envi-met.info/doku.php?id=root:start> (accessed on 27 August 2018).
32. Chatzidimitriou, A.; Yannas, S. Street canyon design and improvement potential for urban open spaces; the influence of canyon aspect ratio and orientation on microclimate and outdoor comfort. *Sustain. Cities Soc.* **2017**, *33*, 85–101. [CrossRef]
33. Jamei, E.; Rajagopalan, P. Urban development and pedestrian thermal comfort in Melbourne. *Sol. Energy* **2017**, *144*, 681–698. [CrossRef]
34. Lee, H.; Mayer, H.; Chen, L. Contribution of trees and grasslands to the mitigation of human heat stress in a residential district of Freiburg, Southwest Germany. *Landsc. Urban Plan.* **2016**, *148*, 37–50. [CrossRef]
35. Fanger, P.O. *Thermal Comfort: Analysis and Applications in Environmental Engineering*; Danish Technical Press: Copenhagen, Denmark, 1970.
36. Jendritzky, G.; Staiger, H.; Bucher, K.; Grätz, A.; Laschewski, G. The perceived temperature: The method of the Deutscher Wetterdienst for the assessment of cold stress and heat load for the human body. In Proceedings of the *Internet Workshop on Windchill*, the Meteorological Service of Canada, Environment Canada, Fredericton, NB, Canada, 3–7 April 2000.
37. Spagnolo, J.; De Dear, R. A field study of thermal comfort in outdoor and semi-outdoor environments in subtropical Sydney Australia. *Build. Environ.* **2003**, *38*, 721–738. [CrossRef]
38. Höppe, P. The physiological equivalent temperature—a universal index for the biometeorological assessment of the thermal environment. *Int. J. Biometeorol.* **1999**, *43*, 71–75. [CrossRef] [PubMed]
39. Brode, P.; Fiala, D.; Blazejczyk, K.; Holmér, I.; Jendritzky, G.; Kampmann, B.; Tinz, B.; Havenith, G. Deriving the operational procedure for the Universal Thermal Climate Index (UTCI). *Int. J. Biometeorol.* **2012**, *56*, 481–494. [CrossRef] [PubMed]
40. Xue, S.; Xiao, Y. Study on the Outdoor Thermal Comfort Threshold of Lingnan Garden in Summer. *Procedia Eng.* **2016**, *169*, 422–430. [CrossRef]
41. Matzarakis, A.; Mayer, H. Another kind of environmental stress: Thermal stress. *WHO Newsl.* **1996**, *18*, 7–10.
42. Knez, I.; Thorsson, S. Influences of culture and environmental attitude on thermal, emotional and perceptual evaluations of a public square. *Int. J. Biometeorol.* **2006**, *50*, 258–268. [CrossRef] [PubMed]
43. Lin, T.-P.; Matzarakis, A. Tourism climate and thermal comfort in Sun Moon Lake, Taiwan. *Int. J. Biometeorol.* **2008**, *52*, 281–290. [CrossRef] [PubMed]
44. Ng, E.; Cheng, V. Urban human thermal comfort in hot and humid Hong Kong. *Energy Build.* **2012**, *55*, 51–65. [CrossRef]
45. Yang, W.; Wong, N.H.; Zhang, G. A comparative analysis of human thermal conditions in outdoor urban spaces in the summer season in Singapore and Changsha, China. *Int. J. Biometeorol.* **2013**, *57*, 895–907. [CrossRef] [PubMed]
46. Charalampopoulos, I.; Tsiros, I.; Chronopoulou-Sereli, A.; Matzarakis, A. A methodology for the evaluation of the human-bioclimate performance of open spaces. *Theor. Appl. Climatol.* **2017**, *128*, 811–820. [CrossRef]
47. Nouri, A.S.; Costa, J.P.; Matzarakis, A. Examining default urban-aspect-ratios and sky-view-factors to identify priorities for thermal-sensitive public space design in hot-summer Mediterranean climates: The Lisbon case. *Build. Environ.* **2017**, *126*, 442–456. [CrossRef]
48. Vardoulakis, S.; Fisher, B.E.; Pericleous, K.; Gonzalez-Flesca, N. Modelling air quality in street canyons: A review. *Atmos. Environ.* **2003**, *37*, 155–182. [CrossRef]
49. Chatzidimitriou, A.; Yannas, S. Microclimate design for open spaces: Ranking urban design effects on pedestrian thermal comfort in summer. *Sustain. Cities Soc.* **2016**, *26*, 27–47. [CrossRef]

50. Liu, Z.; Zheng, S.; Zhao, L. Evaluation of the ENVI-Met Vegetation Model of Four Common Tree Species in a Subtropical Hot-Humid Area. *Atmosphere* **2018**, *9*, 198. [[CrossRef](#)]
51. Yang, X.; Zhao, L.; Bruse, M.; Meng, Q. Evaluation of a microclimate model for predicting the thermal behavior of different ground surfaces. *Build. Environ.* **2013**, *60*, 93–104. [[CrossRef](#)]
52. Rodríguez Algeciras, J.A.; Gómez Consuegra, L.; Matzarakis, A. Spatial-temporal study on the effects of urban street configurations on human thermal comfort in the world heritage city of Camagüey-Cuba. *Build. Environ.* **2016**, *101*, 85–101. [[CrossRef](#)]
53. Morakinyo, T.E.; Kong, L.; Lau, K.K.-L.; Yuan, C.; Ng, E. A study on the impact of shadow-cast and tree species on in-canyon and neighborhood's thermal comfort. *Build. Environ.* **2017**, 115. [[CrossRef](#)]
54. Wen, C.-Y.; Juan, Y.-H.; Yang, A.-S. Enhancement of city breathability with half open spaces in ideal urban street canyons. *Build. Environ.* **2017**, *112*, 322–336. [[CrossRef](#)]
55. Zheng, B.; Bernard Bedra, K.; Zheng, J.; Wang, G. Combination of Tree Configuration with Street Configuration for Thermal Comfort Optimization under Extreme Summer Conditions in the Urban Center of Shantou City, China. *Sustainability* **2018**, *10*, 4192. [[CrossRef](#)]
56. Santamouris, M. Using cool pavements as a mitigation strategy to fight urban heat island—A review of the actual developments. *Renew. Sustain. Energy Rev.* **2013**, *26*, 224–240. [[CrossRef](#)]
57. Qaid, A.; Ossen, D.R. Effect of asymmetrical street aspect ratios on microclimates in hot, humid regions. *Int. J. Biometeorol.* **2015**, *59*, 657–677. [[CrossRef](#)] [[PubMed](#)]
58. Krüger, E.L.; Minella, F.O.; Rasia, F. Impact of urban geometry on outdoor thermal comfort and air quality from field measurements in Curitiba, Brazil. *Build. Environ.* **2011**, *46*, 621–634. [[CrossRef](#)]
59. Sharmin, T.; Steemers, K.; Matzarakis, A. Microclimatic modelling in assessing the impact of urban geometry on urban thermal environment. *Sustain. Cities Soc.* **2017**, *34*, 293–308. [[CrossRef](#)]
60. Huttner, S. *Further Development and Application of the 3D Microclimate Simulation ENVI-met*; Johannes Gutenberg University Mainz: Mainz, Germany, 2012.



© 2019 by the authors. Licensee MDPI, Basel, Switzerland. This article is an open access article distributed under the terms and conditions of the Creative Commons Attribution (CC BY) license (<http://creativecommons.org/licenses/by/4.0/>).